Earth Planets Space, **59**, 841–851, 2007

Early Miocene magnetostratigraphy and a new palaeomagnetic pole position from New Zealand

Gillian M. Turner[1], Daniel M. Michalk[2*], Hugh E. G. Morgans[3], and Jan O. Walbrecker[2†]

[1]*School of Chemical and Physical Sciences, Victoria University of Wellington, P.O. Box 600, Wellington, New Zealand*
[2]*School of Earth Sciences, Victoria University of Wellington, P.O. Box 600, Wellington, New Zealand*
[3]*GNS Science, P.O. Box 30368, Lower Hutt, New Zealand*

(Received October 9, 2006; Revised February 12, 2007; Accepted February 13, 2007; Online published July 20, 2007)

We report palaeomagnetic results from a 26.5 m sequence of early Miocene sediments in NW Nelson, New Zealand. Analysis of the strong, stable characteristic component of natural remanent magnetization has yielded an important record of the part of Chron 5 from ca. 18.5 to 16.5 Ma, including positive identification of the cryptochron or "tiny wiggle" C5Dr-1, and a pole position ($\lambda_p = 78.4^\circ$; $\phi_p = 283.0^\circ$; $dp = 2.2^\circ$; $dm = 2.8^\circ$) for NW Nelson that is indistinguishable from the contemporaneous published pole for the Australian Plate. We infer that this portion of NW Nelson has undergone negligible rotation with respect to the main part of the Australian Plate over the past 17.5 Myr.

Key words: Palaeomagnetism, magnetostratigraphy, Miocene, cryptochron, palaeomagnetic pole position.

1. Introduction

New Zealand has some of the most complete and accessible Cenozoic stratigraphic records in the world. The North Island of New Zealand lies on the Australian tectonic plate, and the Pacific Plate subducts beneath it at an average rate of 45 mm/yr along the Hikurangi Margin. The plate boundary continues through the length of the present-day South Island along the predominantly strike-slip Alpine Fault (Fig. 1(a)). Following the opening of the Tasman Sea, which was complete by about 50 Ma, the plate boundary zone in the region of New Zealand began to evolve dramatically in mid-late Eocene times (Sutherland, 1999). Evidence for this tectonic development include a total dextral offset of 440–470 km on the Alpine Fault, and an apparent bending of the basement terranes found along the length of the country. King (2000) has developed a tectonic model of crustal movements over the past 40 Myr, culminating in the present day configuration of the New Zealand land mass. He divides the New Zealand land mass into 5 tectonic blocks: NW Nelson lies on the Northland—Taranaki—western South Island block, which has remained intact with the Australian Plate while the other blocks have assembled on its eastern margin. King's reconstruction for 18 Ma, the approximate time of deposition of the Tarakohe Mudstone studied here, is shown in Fig. 1(b). Tectonic uplift during the past approximately 5 million years has raised thick sequences of Neogene and Palaeogene marine sediments in many parts of the country, and, these have been the focus of numerous biostratigraphic and magnetostratigraphic studies (e.g. Kennett and Watkins, 1974; Roberts *et al*., 1994; Turner *et al*., 2005), as well as providing indications of the rotation of various crustal blocks and micro-blocks about vertical axes (e.g. Walcott, 1989; Roberts, 1995; Little and Roberts, 1997). The quality of the palaeomagnetic data obtained has however not always been ideal: often the intensity of natural remanent magnetization (NRM) is very weak and a number of factors make it difficult to isolate and determine the primary, detrital component of magnetization (e.g. Roberts and Turner, 1993; Wilson and Roberts, 1999; Turner, 2001). The sequence of early Miocene sediments described here seems to have escaped these problems: the NRM is typically an order of magnitude more intense than that found in other New Zealand mudstones, and comprises an easily removed viscous component overlying a stable characteristic component. The polarity of the characteristic component is unequivocal, except in samples that clearly represent polarity transitions, and the direction is generally very well resolved. In this paper we report the magneto- and bio-stratigraphy of the section, and tectonic implications.

2. Site Description, Sampling

Tarakohe Quarry (latitude 40.83°S, longitude 172.90°E) is on the north coast of the South Island, about 60 km west of Nelson city and 7 km north east of the township of Takaka. A 26.5 m thick section of the early-mid Miocene Tarakohe Mudstone overlies the Takaka Limestone, and is well exposed due to quarrying operations (Figs. 2 and 4(a)). The lowermost unit is a 2 m-thick, hard calcareous siltstone that contains many well-preserved polyzoans, brachiopods and pelecypods. The base of our elevation scale is at the top of this bed, which forms a substantial platform from which to work. The remainder of the section is a massive

*Now at GeoForschungszentrumPotsdam, D-14473 Potsdam, Germany.
†Now at ETH Zurich, CH-8093 Zurich, Switzerland.

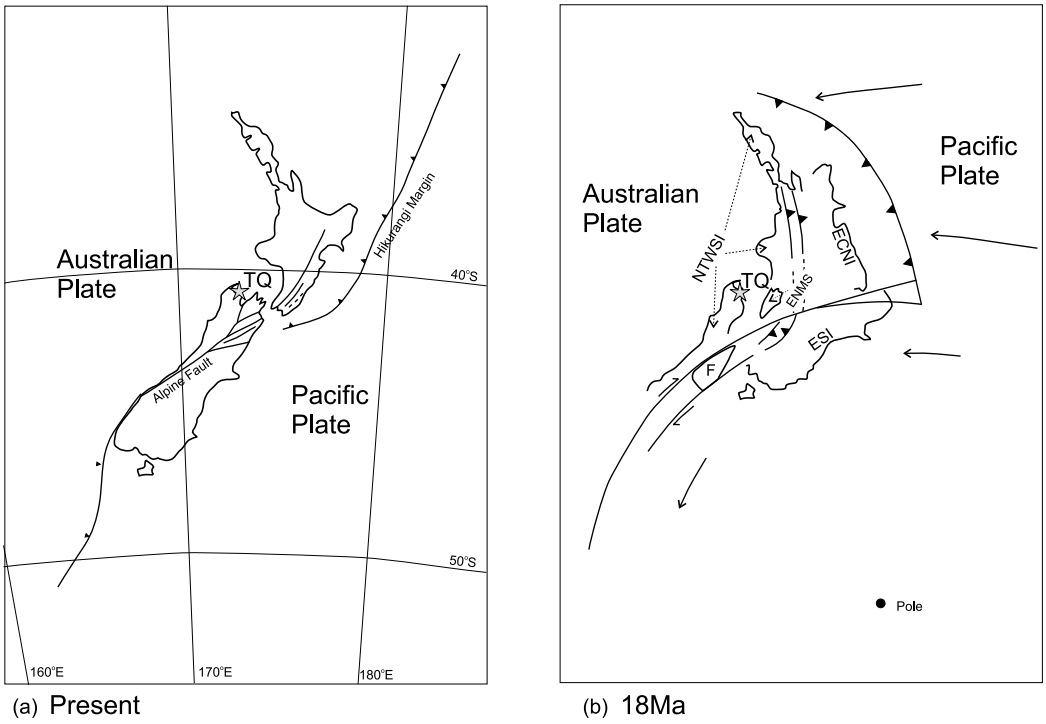

Fig. 1. (a) Present day tectonic map of New Zealand, showing the Alpine Fault associated faults and the Hikurangi Margin which delineate the present-day plate boundary zone. The location of Tarakohe Quarry (TQ) is shown by a star. (b) Tectonic reconstruction of New Zealand, 18 Ma. The five independent rigid crustal blocks employed in the model of King (2000) are Northland-Taranaki-western South Island (NTWSI), East Coast North Island (ECNI), east Nelson Marlborough Sounds (ENMS), eastern South Island (ESI) and Fiordland (F) (after King, 2000).

Fig. 2. Tarakohe Mudstone section at Tarakohe Quarry. The part of the section shown here measures 25 m. The platform in the foreground is the top of the calcareous siltstone that overlies the Takaka Limestone. The lower ca. 5.5 m of massive mudstone is partly covered by vegetation here; it is overlain by a ca. 10 m turbidite sequence, and a further ca. 10 m of silty mudstone. The sampling was carried out in more easily accessible sections nearby.

blue-grey marly mudstone with the exception of an interval of turbidites between 5.5 m and 15.5 m, which consists of harder sandy siltstones between layers and lenses of silty mudstone. The beds are essentially horizontal.

The results presented here are from three suites of samples: two taken at a reconnaissance level and one taken at a closer sampling interval in order to locate the polarity reversals more precisely. All samples were taken with a 2.2 cm diameter, diamond-tipped, water-cooled portable drill, and oriented with a magnetic compass and inclinometer. Horizons TQ00 to TQ09 were sampled by Michalk (2004), as part of a palaeomagnetic investigation of tectonic rotations in the region. They span the lowermost 12 m of the section. Between 2 and 4 samples were drilled from each horizon, and these are distinguished by the third digit of the sample code (e.g. TQ091). A similar strategy was employed for the later sampling of horizons TQ41–TQ47 in the upper part of the section, and TQ60–TQ64 between 5.50 and 2.75 m. The results from these samples have revealed a total of six polarity reversals in the entire section. Subsequent sampling has so far focussed on the three earliest reversals, which occur in the lowermost 3 metres of the section (Walbrecker, 2005). Samples TQ147–242 and 298–300 were drilled at 2–3 cm intervals through this interval. Individual specimens cut from core samples are designated by a letter following the sample code (e.g. TQ091A). The stratigraphic positions of all samples are indicated on Fig. 3(e).

3. Age Control

Macrofossils in the basal calcareous siltstone of the Tarakohe Mudstone were assigned an Altonian age by Fleming (1970) who also considered them to represent moderately deep-water. Foraminifera have been extracted from eleven horizons in the section (Fig. 3(b)) and examined to provide further age control and to estimate the ac-

Table 1. Electron Microprobe elemental analyses of grains identified in Fig. 7. (a) as equivalent oxide percentages, with FeO:Fe_2O_3 correction (Stormer, 1983); (b) as numbers of cations per unit cell (per 32 oxygen ions for inverse spinel structured minerals, per 6 oxygen ions for rhombohedral haematite).

(a)	Grain 1		Grain 2		Grain 3		Grain 4		Grain 6		Grain 5.1		Grain 5.2		Grain 7	
	mass %		mass %		mass %		mass %		mass %		mass %		mass %		mass %	
SiO_2	0.01		0.08		0.00		0.04		0.62		0.00		0.13		0.03	
TiO_2	0.13		0.22		0.09		0.10		0.01		0.10		0.59		47.20	
Al_2O_3	0.05		0.40		0.07		0.24		0.09		22.01		2.89		0.00	
FeO	30.78		30.81		30.49		30.43		31.54		20.93		26.48		37.56	
Fe_2O_3	68.47		67.05		68.55		67.54		67.58		6.12		34.20		8.38	
MnO	0.02		0.03		0.31		0.01		0.08		0.28		3.24		1.29	
MgO	0.00		0.01		0.00		0.00		0.08		8.60		0.56		1.94	
CaO	0.21		0.07		0.05		0.15		0.13		0.06		0.10		0.06	
Cr_2O_3	0.19		0.10		0.07		0.02		0.04		39.47		27.79		0.00	
NiO	0.00		0.00		0.00		0.00		0.00		0.00		0.00		0.00	
ZnO	0.14		0.15		0.25		0.24		0.06		0.54		1.18		0.09	
Total	100.00		98.92		99.88		98.77		100.23		98.11		97.16		96.55	
	spinel		spinel		spinel		spinel		spinel		spinel		spinel		rhombohedral	
(b)	cations per 32 O's	tri-/di-valent ions	cations per 32 O's	tri-/di-valent ions	cations per 32 O's	tri-/di-valent ions	cations per 32 O's	tri-/di-valent ions	cations per 32 O's	tri-/di-valent ions	cations per 32 O's	tri-/di-valent ions	cations per 32 O's	tri-/di-valent ions	cations per 6 O's ilmenite)	*x* (molar fraction)
Si^{4+}	0.00		0.02		0.00		0.01		0.19		0.00		0.04		0.00	
Ti^{4+}	0.03		0.05		0.02		0.02		0.00		0.02		0.14		1.84	
Al^{3+}	0.02	15.97	0.15	15.92	0.03	15.98	0.09	15.96	0.03	15.81	6.71	15.98	1.04	15.82	0.00	
Cr^{3+}	0.05		0.02		0.02		0.00		0.01		8.07		6.73		0.00	
Fe^{3+}	15.87		15.68		15.92		15.84		15.57		1.19		7.88		0.33	
Fe^{2+}	7.93	8.03	8.01	8.08	7.87	8.02	7.93	8.04	8.08	8.19	4.53	8.02	6.78	8.18	1.62	0.92
Mn^{2+}	0.01		0.01		0.08		0.00		0.02		0.06		0.84		0.06	
Mg^{2+}	0.00		0.00		0.00		0.00		0.04		3.31		0.26		0.15	
Ca^{2+}	0.07		0.02		0.02		0.05		0.04		0.02		0.03		0.00	
Ni^{2+}	0.00		0.00		0.00		0.00		0.00		0.00		0.00		0.00	
Zn^{2+}	0.03		0.03		0.06		0.06		0.01		0.10		0.27		0.00	
Total	24.00		24.00		24.00		24.00		24.00		24.00		24.00		4.00	
	magnetite Fe_3O_4		magnetite Fe_3O_4		magnetite Fe_3O_4		magnetite Fe_3O_4		magnetite Fe_3O_4		ferroan chromian spinel $(Cr,Al)_2(Fe,Mg)O_4$		chromian magnetite $(Cr,Fe)_2FeO_4$		ilmeno-haematite $(FeTiO_3)_{0.92}.(Fe_2O_3)_{0.08}$	

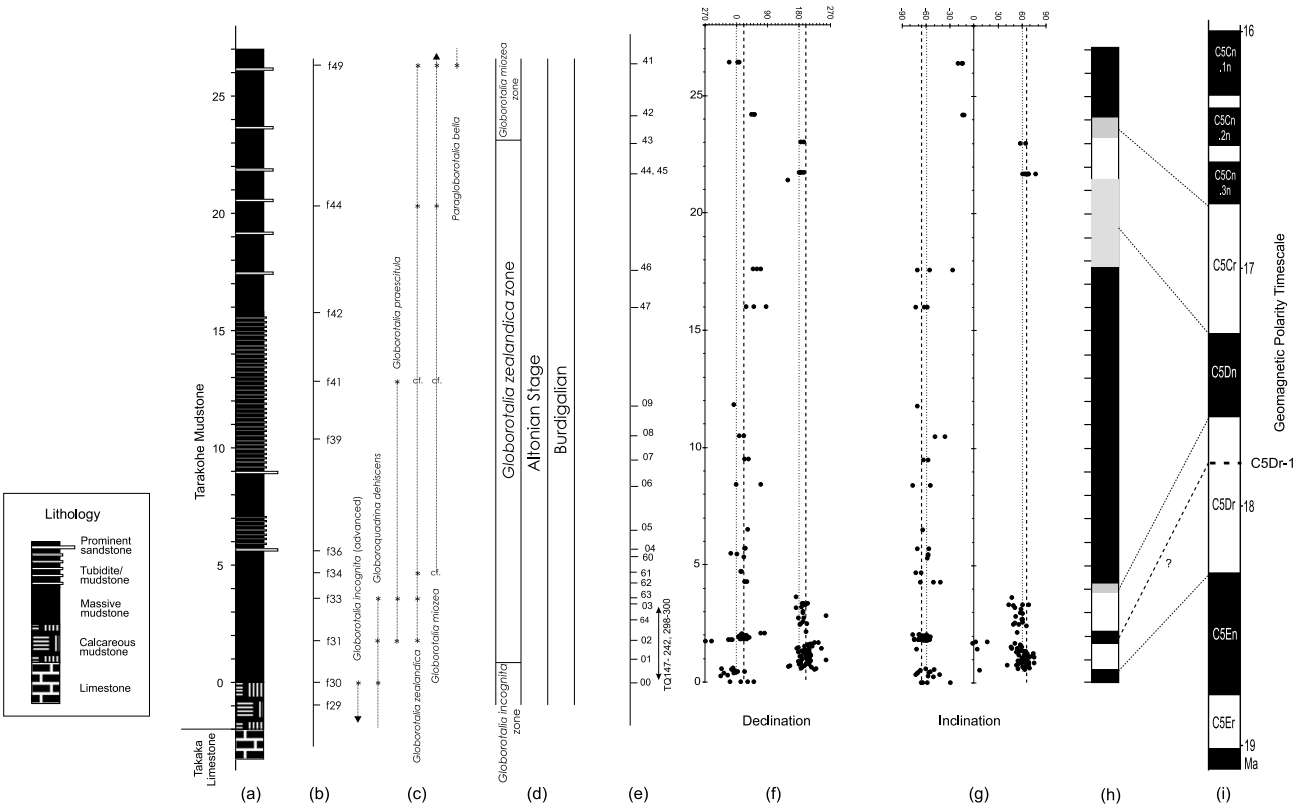

Fig. 3. Stratigraphic records showing (a) lithology; (b) elevations of biostratigraphic samples; (c) planktic foraminiferal biostratigraphy: $*$ = denotes positive identification, cf. = close to the named taxon, but with slight difference: cannot be confidently named; (d) New Zealand stage and zonal scheme; (e) elevations of palaeomagnetic samples; (f) declination and (g) inclination of the characteristic component of NRM. Dotted and dashed lines show the geocentric axial dipole field direction before and after allowance has been made for tectonic movement of the Australian Plate (see text for details); (h) inferred magnetostratigraphy: black = normal polarity, white = reversed polarity, grey = indeterminate polarity (i.e. no samples); (i) proposed correlation with the geomagnetic polarity timescale of Cande and Kent (1995).

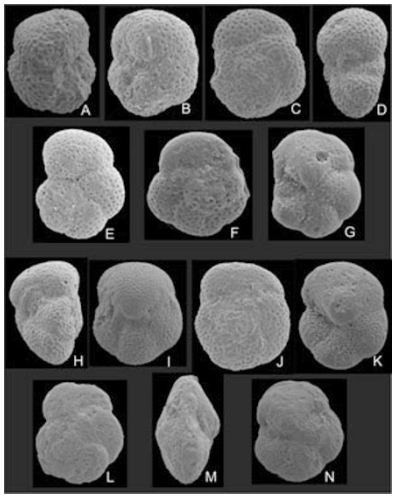

Fig. 4. Planktic foraminifera from Tarakohe Quarry, SEM micrographs. N25/fxx = sample locality (see Fig. 3). FPxxxx = catalogue number of specimen in foraminiferal collection at GNS Sciences, Lower Hutt, New Zealand. A, *Globoquadrina dehiscens* (N25/f30; FP5063). B–D, *Globorotalia incognita*: B, (N25/f30; FP5064); C, (N25/f30; FP5065); D, (N25/f30; FP5066). E. *Paragloborotalia bella* (N25/f49; FP5067). F,G, *Globorotalia praescitula*: F, (N25/f31; FP5068); G, (N25/f31; FP5069). H-J, *Globorotalia zealandica*: H, (N25/f31; FP5070); I, (N25/f31; FP5071); J. (N25/f31; FP5072). K, Specimen transitional between *Globorotalia praescitula* and *G. miozea* (N25/f41; FP5073). L-N, *Globorotalia miozea*: L, (N25/f49; FP5074); M, (N25/f49; FP5075); N, (N25/f49; FP5076).

cumulation rate of the mudstone. Biostratigraphic samples are labelled with Geological Society of New Zealand Fossil Record File locality numbers, NZMS metric sheet N25. Most samples yielded abundant quantities of foraminifera.

The Altonian Stage was subdivided into three planktic foraminiferal zones by Scott (1992), the lower Altonian (*Globorotalia incognita* zone) is represented by the interval from the base of the stage to the entry of *Globorotalia zealandica*. The lowest sample examined in the section (f29) from the hard layer at the top of the limestone yielded no biostratigraphically useful taxa. Samples (f30, f30A) from the top of the calcareous unit and the base of the mudstone respectively, contain forms transitional from *Globorotalia incognita* to *Globorotalia zealandica*, but most likely referable to *Globorotalia incognita* (Fig. 4(B)–(D)) and we suggest this horizon represents the uppermost part of the *Globorotalia incognita* zone, lower Altonian, consistent with the macrofossil evidence. Sample f31, 1.8 m higher, contains a well developed *Globorotalia zealandica* assemblage (Fig. 4(H)–(J)) and is considered the base of the *Globorotalia zealandica* zone (mid Altonian). *Globorotalia zealandica* is present in samples f33, f34, f41, f44, and f49 where it is sparse and small.

The presence of *Globoquadrina dehiscens* (Fig. 4(A)), which disappears from the New Zealand region in the lower *Globorotalia zealandica* zone (Scott, 1992) also supports a mid Altonian age. Morgans *et al.* (2002) place the base of

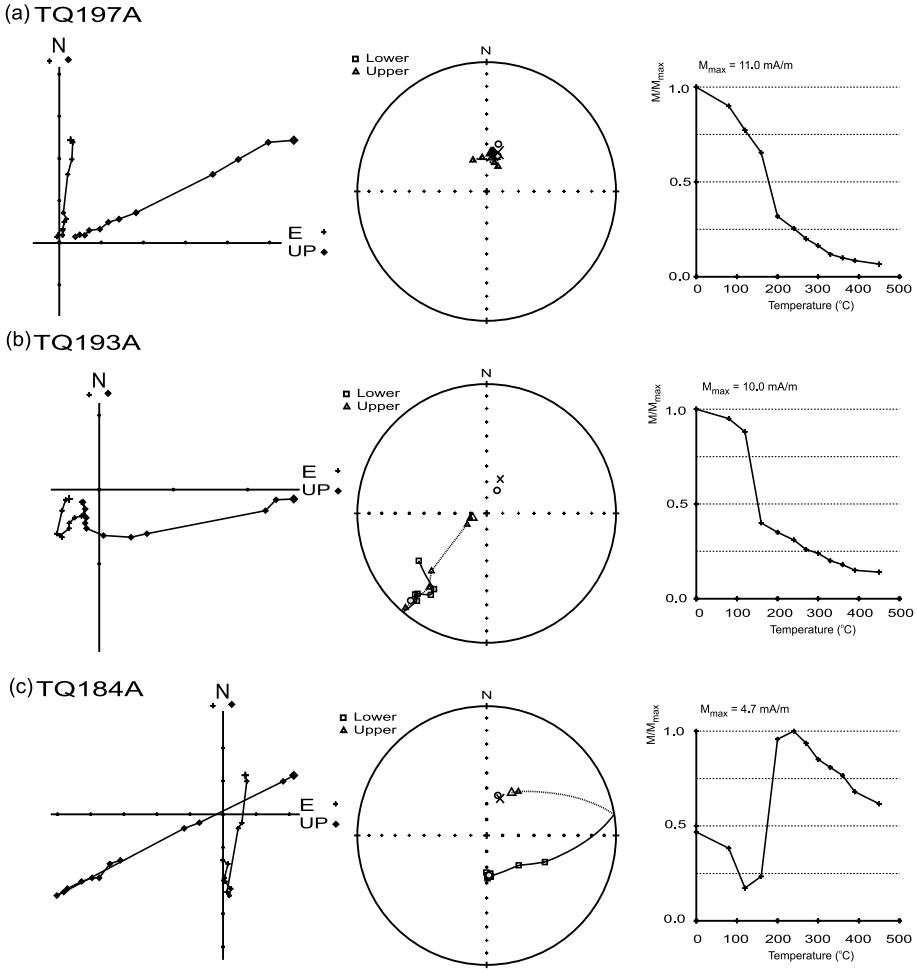

Fig. 5. Progressive thermal demagnetization data of three representative specimens. The left hand diagrams are vector component (Zijderveld) plots: north vs. east (crosses) and north vs. upward (diamonds) components. The centre diagrams are stereographic projections: lower and upper hemisphere directions as squares and triangles respectively. In each case the open white circle shows the secondary component removed (close to the present day field direction, shown by a cross) and the grey dot shows the direction of the characteristic component, interpreted as primary. The right hand diagrams show normalized intensity of magnetization vs. demagnetizing temperature. Specimens TQ 197A, TQ193A and TQ184A have characteristic components of normal, intermediate (transitional?) and reversed polarity respectively.

the *Globorotalia zealandica* zone in Chron C5En (18.781–18.281 Ma). Rare *Globorotalia praescitula* (Fig. 4(F), (G)) were recovered from samples f31, f33 and f41. The overlap of *Globorotalia praescitula* with its presumed descendent *Globorotalia miozea* (Scott *et al*., 1990) occurs in samples f34 and f41, with sparse populations of both taxa. Discrimination between *Globorotalia miozea* and *Globorotalia praescitula* is difficult in the lower 2 samples (Fig. 3(K)). More abundant and typical populations of *Globorotalia miozea* (Fig. 4(L)–(N)) were recovered in the upper 2 samples (f44, f49) where 44% and 48%, respectively, of the specimens were sinistrally coiled. Scott (1992) reports *Globorotalia zealandica* having sub-equal coiling ratios in the lower part of the *Globorotalia miozea* zone (upper Altonian) at DSDP Site 593. A few specimens of *Paragloborotalia bella* (Fig. 4(E)) occur in the uppermost sample (f49). It is possible that the uppermost sample (f49), with well developed *Globorotalia miozea* and rare small *Globorotalia zealandica* is near the top of the *Globorotalia zealandica* zone, possibly just into the *Globorotalia miozea* zone (upper Altonian). This is supported by the continued absence of *Globoquadrina dehiscens*. Berggren *et al*. (1995) place the base of the *Globorotalia miozea* zone at the beginning of C5Cn (ca. 16.726 Ma).

Samples f36, f39, f42 from finer beds within the turbidite intervals, yielded very few, small foraminifera. The planktic component of these faunas lacked key globorotalids. The absence of large sized foraminifers in these samples may be a result of winnowing during turbidite deposition.

The Tarakohe mudstone is therefore assumed to be mainly mid-Altonian in age (*Globorotalia zealandica* zone). The 26.5 m section sampled spans an interval of approximately 2.0 million years, from which we infer an average accumulation rate of about 13 m per million years. This is extremely slow compared with other New Zealand mudstone sequences, some of which accumulated 10 or 100 times faster (e.g. between 1 and 2 m per thousand years in Wanganui Basin, Turner *et al*., 2005).

4. Magnetic Properties of the Sediments

4.1 Stability of the natural remanent magnetization

Although the average magnetic susceptibility of 750 $\times$ 10^{-6} SI is fairly typical of New Zealand mudstones, the average intensity of NRM, 10 mA·m^{-1} (range 1–30 mA·m^{-1}),

is an order of magnitude stronger.

Progressive demagnetizion was carried out to investigate the nature of the remanent magnetization. Preliminary tests showed that, as in previous studies on similar material (e.g. Roberts *et al.*, 1994; Turner *et al.*, 2005), thermal demagnetization was effective at separating the various components of NRM, while alternating field (AF) techniques were not, being often affected by the introduction of spurious magnetizations. No further AF demagnetization was conducted. Most thermal demagnetization and remanence measurements were carried out at the Black Mountain Laboratory of the Australian National University using a large-volume furnace enclosed in a field-cancelling system of Helmholtz coils and an SCT 3-axis cryogenic magnetometer with a sensitivity better than 10^{-11} A.m^2. A subset of specimens was analysed using comparable equipment at Ludwig-Maximilians University, Munich.

At least one specimen from each sample was thermally demagnetized at temperatures of 80, 120, 160, 200, 240, 270, 300, 330 and 360°C. Many New Zealand Neogene mudstones undergo thermal alteration to the magnetic mineralogy between about 300 and 400°C, causing large increases in magnetic susceptibility and the development of anomalous, often viscous components of magnetization. Most Tarakohe Quarry samples however remained stable, and progressive demagnetization was continued: in some cases to 600°C, at which point a small but measurable remanence still persisted. Vector component, stereographic and normalized intensity plots of the demagnetization data of some typical specimens are shown in Fig. 5. All specimens carry a substantial viscous component of magnetization, which is removed by demagnetization to about 200°C. In all cases this viscous component is very close to the present day geomagnetic field at Tarakohe Quarry: $Dec = 21.4°$, $Inc = -66.5°$. It is underlain by a stable component that, on further demagnetization, trends linearly towards the origin of a vector component plot. This characteristic component (ChRM) is interpreted as the primary, detrital component of magnetization. In specimen TQ197A it is of normal polarity ($Dec = 12.2°$; $Inc = -68.5°$; maximum angular deviation (MAD) $= 2.4°$), and is close to the viscous component, necessitating care in distinguishing it. Comparison of the blocking temperature spectrum with the plots of remanent intensity vs. temperature for the other specimens does however suggest two components. In specimen TQ184A the ChRM is of reversed polarity ($Dec = 176.8°$; $Inc = 64.4°$; $MAD = 1.4°$), while in specimen TQ193A, it is very shallow, and to the south west, ($Dec = 224.7°$; $Inc = -2.4°$; $MAD = 11.2°$), and is an example of a transitional direction recorded during a polarity reversal. Transitional directions are difficult to isolate and resolve because of the weak intensity of the ChRM (possibly due to a weak transitional palaeointensity). However there is a very marked contrast between the demagnetization behaviours of these specimens and stable normal and reversed polarity specimens stratigraphically above and below them.

4.2 Nature of the remanence carriers

As mentioned previously, these strong, stable two-component magnetizations are relatively unusual in New Zealand mudstones. In many other studies, a third, high blocking temperature component has been found, which seems to be secondary in origin and to overprint and partially or completely replace the primary magnetization (Turner, 2001). Investigations of the magnetic mineralogy were therefore carried out to look for any significant difference between the TQ sediments and those of previous studies.

In the experiments described below, isothermal remanent magnetizations (IRM's) were grown using a Molspin pulse magnetizer and measured using a Molspin "Minispin" fluxgate spinner magnetometer. Bartington MS2 instrumentation, including a small volume (1–2 cm^3) furnace was used to investigate the temperature dependence of magnetic susceptibility. The Victoria University scanning electron microscope, with JEOL 773 electron microprobe, was used to obtain estimates of elemental composition of selected magnetic grains. Where extracted magnetic grains have been studied rather than whole sediment samples, these grains have been obtained from dried disseminated sediment with a hand magnet. For some of the IRM experiments, such grains were mounted in plaster of paris to make standard-sized cylindrical "specimens".

In Fig. 6(a) we show the results of progressive acquisition of IRM in a typical specimen, followed by application of fields of increasing magnitude in the opposite direction. The IRM saturates between 200 and 400 mT, with a coercivity of back IRM (B_{cr}) of 41 mT: these values are characteristic of low coercivity ferrimagnetic minerals such as (titano-)magnetite, maghaemite, and greigite. There is no evidence of a high coercivity component. The plot of magnetic susceptibility against temperature shown in Fig. 6(b) was obtained from a sample of extracted magnetic grains. The main reversible change occurs at about 570°C, and this is interpreted as the Curie temperature of the main ferrimagnetic phase. There is also an irreversible decrease of susceptibility at about 350°C, and a small signal remaining above the main Curie temperature, finally vanishing at about 620°C. Similar results were obtained from grains extracted from the lower (0.36–1.07 m), middle (1.70–1.85 m) and upper (16–26 m) parts of the section.

In Fig. 6(c) we show thermal (un)blocking spectra of IRM's carried by the low, mid and high coercivity components of the grain distribution, for a representative specimen. Following the technique described by Lowrie (1990), an IRM was first grown in a field of 1.000 T along the z axis of the specimen (in this case, an electromagnet was used to impart the IRM, in order to maximise the field obtainable). IRM's were subsequently grown in fields of 400 mT and 100 mT along the y and x axes respectively. This was repeated for specimens from the lower, mid and upper part of the section. We also treated plaster of paris mounted samples of extracted grains, and a blank specimen of plaster of paris, in order to check for possible fractionation or anomalies brought about in the extraction process. After initial measurement of the IRM components, all specimens were thermally demagnetized at 100°C and then at intervals of 50°C up to 650°C.

The IRM components of the blank were found to be less than 1% of those of the whole sediment specimens, and less than 10% of those of the specimens containing extract. A

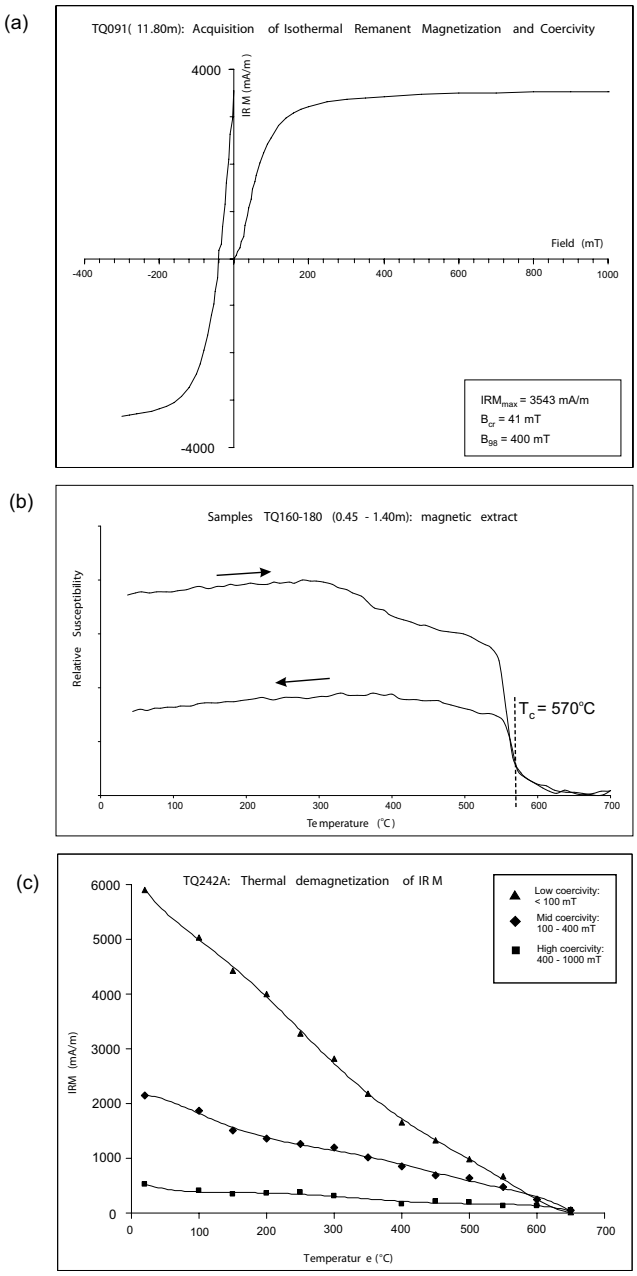

Fig. 6. (a) Acquisition of isothermal remanent magnetization (IRM) and back IRM data for specimen TQ091 (turbidites), showing a low coercivity (B_{cr} = coercivity of back IRM = 41 mT) and low-field saturation (B_{98} = field at which 98% of saturation IRM is reached = 400 mT), typical of ferrimagnetic minerals such as (titano-) magnetite. (b) Variation of magnetic susceptibility with temperature for a sample of grains extracted from elevations between 0.45 and 1.40 m. The upper curve is the heating and the lower curve the cooling process. There is a slight irreversible loss of susceptibility at about 350°C, a clear Curie temperature at 570°C, and possibly a small residual magnetic component to ca. 620°C. (c) Thermal demagnetization of low (<100 mT), mid (100–400 mT) and high (400 mT–1 T) coercivity IRMs grown along orthogonal directions in specimen TQ242A (3.33 m).

correction was made to the data from the extracts.

In all cases the low coercivity component dominated the IRM, while the high coercivity component was scarcely significant. For the whole sediment specimens the ratios of low (<100 mT) to mid (100–400 mT) to high (400 mT–1 T) components were 1.00:0.27 (±0.06):0.09 (±0.03),

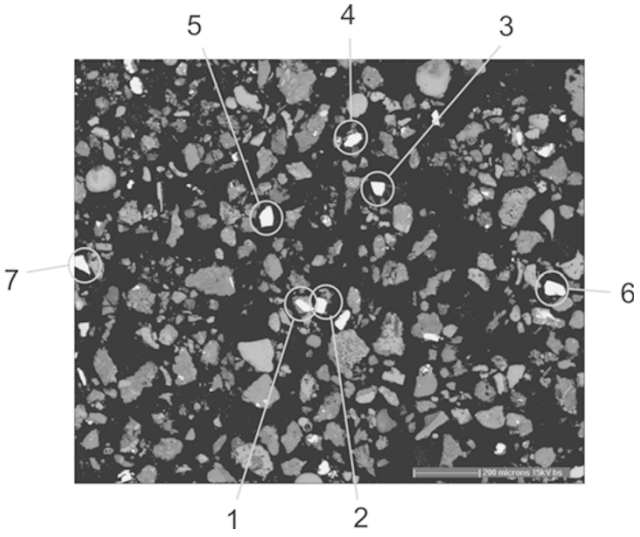

Fig. 7. Wide angle scanning electron microscope image of grains extracted with a hand magnet from dried sediment from samples between TQ160 and TQ180 (0.5–1.5 m). White (highly reflective) grains indicated are those for which electron microprobe analyses are given in Table 1.

while for the extracts the ratios were 1.00:0.14 (±0.01):0.02 (±0.01). In general, the low and mid coercivity components demagnetize to a Curie temperature between 550° and 600°C, with a small contribution persisting to the final 650°C step, in accord with the results of demagnetization of the NRM, and the susceptibility vs. temperature experiments. In the extract specimens, but less noticeable in the whole sediment specimens, is the suggestion of a lower unblocking temperature, at about 400°C, especially in the low coercivity curve.

Both whole sediment thin sections and mounted samples of grains extracted by hand magnet were examined under optical and electron microscopes. Figure 7 is a wide-view scanning electron microscope image, in which the ferrimagnetic grains show up as the bright white grains. Electron microprobe compositional analyses of the grains circled in Fig. 7 are detailed in Table 1. Table 1(a) contains equivalent oxide percentages, with FeO and Fe_2O_3 percentages calculated to eliminate charge deficiency or excess (Stormer, 1983), while Table 1(b) lists the number of each metal cation per unit cell: 32 oxygen anions for a spinel crystal structure or six for a rhombohedral crystal.

Grains 1, 2, 3, 4 and 6 are all almost pure magnetite ($Fe_2^{3+}Fe^{2+}O_4$), with excellent total percentages, and an average Fe^{3+}:Fe^{2+} ratio of 1.97 ± 0.02.

Grain 5 is typical of several grains analysed in each of the slides examined. It yields a good spinel composition, including Fe^{3+} and Fe^{2+}, but with significant proportions of Fe^{3+} substituted with Al^{3+} and Cr^{3+} in the place of Fe^{3+}, and significant proportions of Fe^{2+} substituted with Mg^{2+} (and to a lesser extent Mn^{2+}) in the place of Fe^{2+}.

Grain 7 is quite different—it is a member of the ilmenite—haematite solid solution series, located very close to the ilmenite end. Ilmenite is a common component of sediments and sands in the west and northwest of the South Island (Deer *et al.*, 1996), but this composition is paramagnetic at room temperature, and so is unlikely to

contribute to the remanent magnetization of the TQ sediments.

Similar results were also obtained from the grains extracted by hand magnet from the middle and upper parts of the section. No iron sulphide grains were found in any of these mounts. A thin section of whole sediment from TQ7 (9.5 m), within the turbidite sequence, was also examined. Microprobe analyses identified several grains of ilmenite, a multiphase chromite grain similar to Grain 5 above, and a single foraminifera cast in which framboidal aggregates of micron-sized, near-stoichiometric pyrite crystals had formed. In none of the samples were any ferrimagnetic iron sulphides e.g. pyrrhotite (Fe_9S_{10}–Fe_7S_8) or greigite (Fe_3S_4) found.

4.3 Discussion

We conclude that, in the main, massive, parts of the section, the principal remanence carrier is near stoichiometric magnetite, as evidenced by the dominant unblocking and Curie temperatures of around 570°C. We believe it is mainly this magnetite that carries the characteristic component of NRM, which is isolated at demagnetization temperatures between 200°C and 580°C. A number of ferrimagnetic minerals have maximum unblocking temperatures between 300 and 400°C: these include greigite and pyrhotite, and titanomagnetites and chromium spinels of appropriate compositions (Dunlop and Ozdemir, 1997). Of these only chromite and chromium spinels are seen in the elemental analsyes: therefore, though unusual, they are considered likely carriers of the 300–400°C component. The small magnetization that persists above 570°C is thought to be due to a cation-deficient (oxidized) form of magnetite—a spinel with composition between magnetite and maghaemite.

Although it is surprising to find a viscous secondary component of NRM extending to unblocking temperatures of 200°C, it is not uncommon in New Zealand Neogene mudstones, and, whereas in other cases it often masks the ChRM, at TQ this is not a problem.

The magnetic properties and inferred mineralogy of the Tarakohe Mudstone presented here are in stark contrast to those of most other New Zealand mudstones (e.g. Roberts and Turner, 1993; Wilson and Roberts, 1999; Hüsing, 2002; Michalk, 2004). In most other cases pyrite is ubiquitous, while pyrrhotite and greigite are common ferrimagnetic minerals. Primary detrital magnetite is rare, and, where present, usually shows evidence of surface-pitting and dissolution. In many such cases the NRM is weak (<1 mA·m^{-1}), and is often difficult to interpret. Frequently the component of magnetization that underlies the viscous component does not demagnetize towards the origin of the vector component plot, suggesting a third, high unblocking temperature component. Isolation and further investigation of this third, overlying component is however almost invariably compromised by thermal alteration of the sample. Turner (2001) and Turner *et al.* (2005) conclude that this behaviour is compatible with reductive dissolution of iron from the detrital oxide mineral, lowering its contribution to the NRM, while forming iron sulphides. If the sulphidization does not reach its endpoint, pyrite (FeS_2), then a secondary component of magnetization may result, carried by fine-grained greigite.

The Tarakohe Mudstone seems to have escaped the anoxic conditions necessary for sulphidic reduction of magnetite. This is evidenced by the absence of greigite, pyrrhotite or pyrite, the presence of fresh detrital magnetite grains and well preserved foraminfera, and the straightforward, two-component nature of the NRM. The reason for this is not completely understood: it is likely to be associated with the slow deposition rate of the massive sediments, presumably in an environment relatively poor in available sulphur.

5. Magnetostratigraphy and Palaeomagnetism

5.1 Results

A total of 130 specimens, one or more from each drilled sample, were thermally demagnetized as described above, and the data analysed using principal component analysis (PCA). In all cases the viscous component is removed by heating to 200°C, and is underlain by a stable component of magnetization, that trends towards the origin of the vector component plot. This component is interpreted as the primary component of NRM. Its direction was generally determined by PCA of data from 240°C upwards: this usually comprised between six and eight demagnetization levels, and yielded a maximum angular deviation (MAD) that was generally less than 5°. The declination and inclination of this component is plotted for each specimen analysed in Fig. 3(f) and (g). Also shown are the declination and inclination expected at the site for a geocentric axial dipole field (i) for no tectonic movement ($D = 0.0°, 180.0°$; $I = \pm 59.9°$), and (ii) if the site has moved coherently with the Australian Plate, as described by Veevers and Li (1991) ($D = 20.0°$, $I = \pm 66.3°$, for 17.5 Ma).

As mentioned previously, the reconnaissance sampling enabled identification of six polarity reversals. Detailed sampling has located the lowermost normal to reversed transition at 0.57 ± 0.05 m, a reversed to normal transition at 1.81 ± 0.05 m, closely followed by another normal to reversed transition at 2.05 ± 0.05 m. Another reversed to normal transition follows between horizons TQ63 and TQ62 (3.63 and 4.28 m). All these transitions occur in the lower massive part of the section below the turbidites. All horizons sampled from fine-grained material within the turbidite sequence carry a normal polarity, as do horizons TQ47, TQ46, TQ42 and TQ41. Horizons TQ45, 44 and 43 however have a reversed polarity, indicating two more reversals in the upper part of the section, between 17.6 and 21.6 m and between 23.0 and 24.2 m.

5.2 Correlation with the GPTS: a record of C5Dr-1

Geomagnetic polarity stratigraphy is shown in Fig. 3(h), to the right of the declination and inclination logs, and alongside (Fig. 3(i)) is the early Miocene part of the geomagnetic polarity timescale (GPTS) of Cande and Kent (1992, 1995). The biostratigraphic age control discussed above suggests correlation of the lowermost normal polarity interval with Chron C5En, by comparison with results from Tangakaka Stream, NE North Island, which are supported by an Ar-Ar age estimate on a key tephra layer (Morgans *et al.*, 2002). This is in accord with the recommendations of Berggren *et al.*, (1995) in their Cenozoic chronostratig-

Table 2. Summary of mean palaeomagnetic directions and pole positions for TQ data, geocentric axial dipole and the Australian apparent polar wander path.

TQ Mean Directions	Declination	Inclination	N	α_{95}	Pole latitude	Pole longitude	dp	dm
Normal	14.5	−64.3	55	2.9				
Reversed	195.8	61.1	65	2.2				
Overall	15.2	−62.5	120	1.8	78.4	283.0	2.2	2.8
	Expected Declination	Expected Inclination						
Geocentric Axial Dipole	0	−59.9			90	—		
Australian APWP*	20	−66.3			74	299		

*Veevers and Li (1991).

raphy and of Cooper (2004) in the New Zealand Geological Timescale. Robust populations of *Globorotalia miozea* first appear near the top of the sequence, in the uppermost reversed interval. Berggren *et al.* (1995) place the first occurrence (FO) of *Globorotalia miozea* at the beginning of C5Cn.3n, on the basis of the magnetobiostratigraphy of cores from ODP Holes 747A and 751A from the Kerguelen Plateau (Berggren, 1992). This correlation, and an age of 16.7 Ma, were adopted by Cooper (2004) as the base of the upper Altonian sub-stage. We therefore correlate the uppermost normal interval with C5Cn.3n, and suggest the FO of *Globorotalia miozea* may be slightly older than earlier studies suggest, perhaps an intra C5Cr event. Further comparison with the GPTS suggests that the long normal polarity interval beginning at about 4 m and extending through the turbidite sequence corresponds to C5Dn. The record of this interval is expanded due to the accelerated accumulation of the turbidites, compared with the massive mudstones above and below. This leaves the question of the identity of the short but well recorded normal polarity interval between 1.81 and 2.05 m. Cande and Kent (1992, 1995) did not resolve any distinct subchrons in this interval, but they did note a "tiny wiggle" in the marine magnetic anomaly records from which this part of the GPTS was constructed (Blakely, 1974), and labelled it cryptochron C5Dr-1. Blakely had previously modelled it as a short zone of normal polarity. Similar features occur throughout the GPTS: although Cande and Kent attribute them to the palaeomagnetic field, they reserve judgement as to whether they represent short polarity intervals, or longer period intensity variations. The uncertainty arises because the smoothed nature of the marine magnetic anomaly record makes it difficult to model such "tiny wiggles" unambiguously. However, the Tarakohe Quarry record presented here is compiled from independent, discrete samples and so is unequivocal. Between 1.81 and 2.05 m, a total of 21 specimens record normal polarity directions, with an average Dec = 12.4°, Inc = −65.3°, α_{95} = 3.4°. At ODP Site 1090, Channell *et al.* (2003) also obtained a clear record of C5Dr-1, as well as records of two older cryptochrons that were absent from the Cande and Kent (1992, 1995) timescale. We estimate that the field established a normal polarity for about 70,000 years, in close agreement with the 55,000 years estimated by Channell *et al.* We therefore support their recommendation to (re-)elevate C5Dr-1 to the status of a subchron: C5Dr.1n.

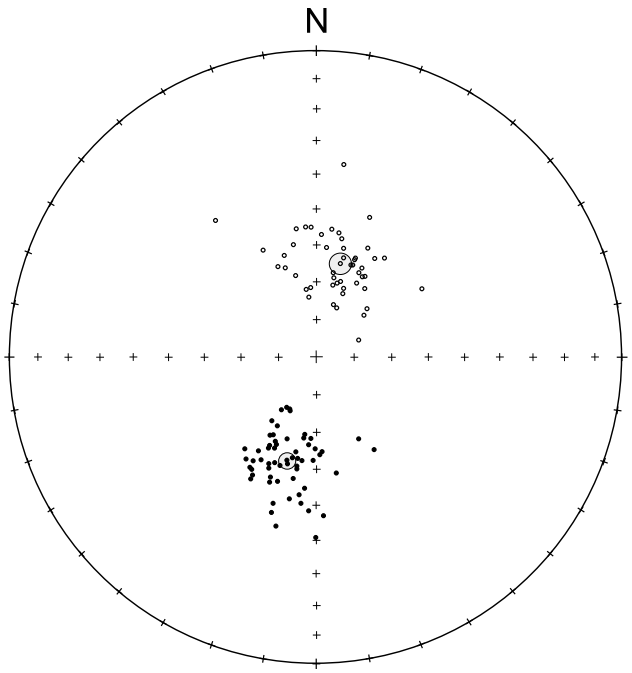

Fig. 8. Equal angle stereographic projection showing directions of the characteristic component of NRM of all specimens. Grey circles show mean normal (D = 14.5°, I = −64.3°, α_{95} = 2.9°, N = 55) and reversed (D = 195.8°, I = 61.1°, α_{95} = 2.2°, N = 65) polarity directions with associated cones of 95% confidence.

5.3 Tectonics: A New Palaeomagnetic Pole Position

The entire set of palaeomagnetic directions is plotted on an equal angle stereographic projection in Fig. 8. The mean directions and corresponding pole positions are summarized in Table 2. The means of the normal polarity and reversed polarity directions are antipodal at the 95% level of confidence: hence the data set passes a reversals test, and we can be satisfied that secondary components of magnetization have been effectively removed, and that secular variation has been adequately sampled and averaged (e.g. Butler, 1992). Averaging the normal polarity directions with the antipodes of the reversed polarity directions yields an overall mean direction of D = 15.2°, I = −62.5°, α_{95} = 1.8°, N = 120.

When averaged over a period long enough to adequately sample secular variation (10^4–10^5 years or more), the ge-

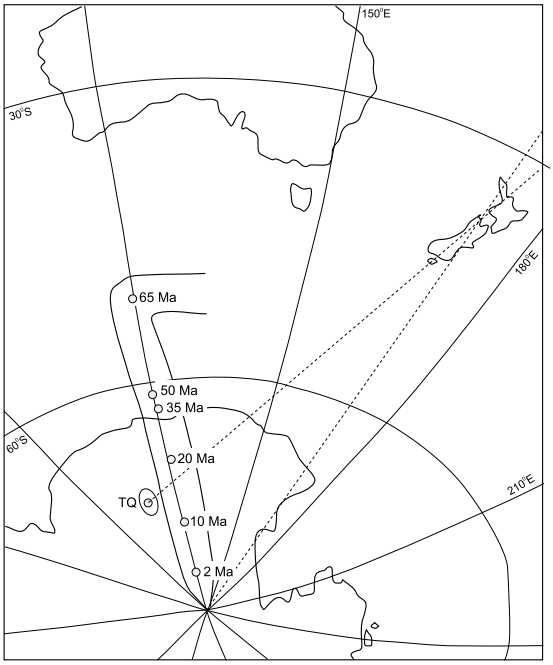

Fig. 9. Apparent polar wander path for Australia for the Cenozoic time period, from Veevers and Li (1991). Also the pole position calculated from TQ data, and its 95% confidence limits.

omagnetic field is generally assumed to closely approximate that of a geocentric axial dipole (GAD). At Tarakohe Quarry a normal GAD would produce a declination of zero, and an inclination of -59.9°. The difference between this and the overall mean direction is interpreted in terms of tectonic movement of the site with respect to the rotation pole since deposition of the sediments. The inclination steepening, $\Delta I = 2.6 \pm 1.8^\circ$, though only just significant, indicates a small northward shift (340 ± 235 km) over the past ca. 17.5 Ma, while the declination anomaly of $15.2^\circ \pm 3.6^\circ$ reflects an overall clockwise rotation. (The symmetry of the geocentric axial dipole field means that overall longitudinal movement cannot be detected).

King (2000), in his tectonic reconstruction of New Zealand over the past 40 Myr, treated NW Nelson, along with the west coast of the South Island, and the Taranaki and Northland peninsulas, as a single block located on the Australian Plate. He divided the remaining landmass into four crustal blocks whose movement he modelled with respect to the Australian Plate (Fig. 1(b)). Our results are in accord with the assignment of NW Nelson to the Australian Plate: they show that the movement of NW Nelson, over at least the past 17.5 Myr has closely mirrored that of the Australian Plate as defined by the Apparent Polar Wander Path (APWP) of Veevers and Li (1991), shown in Fig. 9. The pole calculated from the mean TQ direction ($\lambda_p = 78.4^\circ$; $\phi_p = 283.0^\circ$) differs from the APWP pole ($\lambda_p = 74^\circ$; $\phi_p = 299^\circ$) by only 5.8°. The APWP pole was calculated by interpolation between poles "estimated at approximately" 12 and 26 Ma (Idnurm, 1985), each of which carried alpha-95's of about 4.5°. The difference between the TQ and APWP poles is therefore not considered significant, and the quality and resolution of the palaeomagnetic data and age control may in fact be superior to those available to Veevers and Li (1991).

If NW Nelson is taken to have been a coherent part of the Australian Plate, then our data yield a new mid Miocene palaeomagnetic (N) pole position: $\lambda_p = 78.4^\circ$; $\phi_p = 283.0^\circ$; $dp = 2.2^\circ$; $dm = 2.8^\circ$; age = 17.5 Ma. (S pole: $\lambda_p = 78.4^\circ$S; $\phi_p = 103.0^\circ$).

6. Conclusions

In this study we have demonstrated that the early Miocene sediments exposed at Tarakohe Quarry carry a stable high quality palaeomagnetic record and foraminiferal assemblage that have not been affected by reductive diagenesis and sulphidization. The magnetostratigraphic record includes six geomagnetic reversals, and has been correlated with the GPTS between C5En and C5Cn (ca. 18.5 to 16.5 Ma). A clear record of the "cryptochron" C5Dr-1 has been retrieved and we support its re-labelling as a subchron. The mean palaeomagnetic direction shows that NW Nelson has moved coherently with the Australian tectonic plate over the past 17.5 Ma, and yields a palaeomagnetic pole position of $\lambda_p = 78.4^\circ$; $\phi_p = 283.0^\circ$; $dp = 2.2^\circ$; $dm = 2.8^\circ$; age = 17.5 Ma.

Acknowledgments. We would like to thank Mr. R. Butts of Takaka for generous access to Tarakohe Quarry; Brad Pillans, Chris Klootwick and the palaeomagnetic group at Australian National University for use of the Black Mountain laboratory and constructive discussions on this work. JOW carried out measurements at the palaeomagnetic facility at Ludwig-Maximilians University, Munich. John Patterson, of VUW School of Earth Sciences provided invaluable expertise with the electron microscope and microprobe analyses. Principal component analysis of the progressive demagnetization data was carried out using R. Enkin's package of programmes for PC's. Fieldwork and measurements were supported by grants from the VUW Faculty of Science. The careful and thoughtful reviews of Drs. C.-S. Horng and H. Hoshi have helped us to improve the manuscript significantly.

References

Berggren, W. A., Neogene planktonic foraminifer magnetobiostratigraphy of the southern Kerguelen Plateau (Sites 747, 748, and 751). Proc. Ocean Drilling Program, *Scientific Results*, **120**, 631–643, 1992.

Berggren, W. A., D. V. Kent, C. C. Swisher III, and M. P. Aubry, A revised Cenozoic geochronology and chronostratigraphy, in *Geochronology, Time Scales and Global Stratigraphic Correlations*, edited by W. A. Berggren, D. V. Kent, M. P. Aubry, and J. Hardenbol, SEPM (Society for Sedimentary Geology) Special Publication 54, 129-212, 1995.

Blakely, R. J., Geomagnetic reversals and crustal spreading rates during the Miocene, *J. Geophys. Res.*, **79**, 2979–2985, 1974.

Butler, R. F., *Paleomagnetism: Magnetic Domains to Geologic Terranes*, 319 pp., Blackwell, Boston, 1992.

Cande, S. C. and D. V. Kent, A new geomagnetic polarity timescale for the late Cretaceous and Cenozoic, *J. Geophys. Res.*, **97**, 13917–13951, 1992.

Cande, S. C. and D. V. Kent, Revised calibration of the geomagnetic polarity timescale of the late Cretaceous and Cenozoic, *J. Geophys. Res.*, **100**, 6093–6095, 1995.

Channell, J. E. T., S. Galeotti, E. E. Martin, K. Billups, H. D. Scher and J. S. Stoner, Eocene to Miocene magnetostratigraphy, biostratigraphy, and chemostratigraphy at ODP Site 1090 (sub-Antarctic South Atlantic), *Geological Society of America Bulletin*, **115**, 607–623, 2003.

Cooper, R. A. (editor), The New Zealand Geological Timescale, 270 pp., *Institute of Geological and Nuclear Sciences Monograph 22*, 2004.

Deer, W. A., R. A. Howie and J. Zussman, *An Introduction to the Rock Forming Minerals*, 2nd edition, 696 pp., Longman, 1992.

Dunlop, D. J. and Ö. Özdemir, *Rock Magnetism: Fundamentals and Fron-*

tiers, 573 pp., Cambridge University Press, 1997

Fleming, C. A., Two new deep-water Mollusca from the Tarakohe Mudstone (Lower Miocene) of Nelson, New Zealand, *New Zealand Journal of Geology and Geophysics*, **13**, 676–683, 1970.

Hüsing, S., Environmental magnetism and remanence acquisition in the cyclic sedimentation in the Eocene-Oligocene at Cape Foulwind. BSc (Hons) thesis, Victoria University of Wellington, New Zealand, 2002.

Idnurm, M., Late Mesozoic and Cenozoic palaeomagnetism of Australia—I. A redetermined apparent polar wander path, *Geophys. J. R. Astr. Soc.*, **83**, 399–418, 1985.

Kennett, J. P. and N. D. Watkins, Late Miocene—Early Pliocene paleomagnetic stratigraphy, paleoclimatology and biostratigraphy in New Zealand, *Bull. Geol. Soc. America*, **85**, 1385–1398, 1974.

King, P. R., Tectonic reconstructions of New Zealand: 40 Ma to the present, *New Zealand Journal of Geology and Geophysics*, **43**, 611–638, 2000.

Little, T. A. and A. P. Roberts, Distribution and mechanism of Neogene to present-day vertical axis rotations, Pacific-Australian plate boundary zone, New Zealand, *J. Geophys. Res.*, **102**(B9), 20447–20468, 1997.

Lowrie, W., Identification of ferromagnetic minerals in a rock by coercivity and unblocking temperature properties, *Geophys. Res. Lett.*, **17**, 159–162, 1990.

Michalk, D. M., Palaeomagnetic studies of Cenozoic sedimentary rocks of the northwest Nelson area, New Zealand, and implications for the tectonic history of the region, MSc thesis, Victoria University of Wellington, New Zealand, 2004.

Morgans, H. E. G., G. H. Scott, A. R. Edwards, I. J. Graham, T. C. Mumme, D. B. Waghorn, and G. S. Wilson, Integrated stratigraphy of the lower Altonian (Early Miocene) sequence at Tangakaka Stream, East Cape, New Zealand, *New Zealand Journal of Geology and Geophysics*, **45**, 145–173, 2002.

Roberts, A. P., Tectonic rotation about the termination of a major strike-slip fault, Marlborough fault system, New Zealand, *Geophys. Res. Lett.*, **22**, 187–190, 1995.

Roberts, A. P. and G. M. Turner, Diagenetic formation of ferrimagnetic iron sulphide minerals in rapidly deposited marine sediments, South Island, New Zealand, *Earth Planet. Sci. Lett.*, **115**, 257–273, 1993.

Roberts, A. P., G. M. Turner, and P. P. Vella, Magnetostratigraphic chronology of late Miocene to early Pliocene biostratigraphic and oceanographic events in New Zealand, *Bull. Geol. Soc. America*, **106**, 665–683, 1994.

Scott, G. H., Planktonic foraminiferal biostratigraphy (Altonian-Tongaporutuan Stages, Miocene) at DSDP Site 593, Challenger Plateau, Tasman Sea, *New Zealand Journal of Geology and Geophysics*, **35**, 501–513, 1992.

Scott, G. H., S. Bishop, and B. J. Burt, Guide to some Neogene globorotalids (Foraminiferida) from New Zealand, *New Zealand Geological Survey Paleontological Bulletin*, **61**, 135 pp., 1990.

Stormer, J. C., The effects of recalculation on estimates of temperature and oxygen fugacity from analyses of multicomponent iron-titanium oxides, *American Mineralogist*, **68**, 586–594, 1983.

Sutherland, R., Cenozoic bending of New Zealand basement terranes and Alpine Fault displacement: a brief review, *New Zealand Journal of Geology and Geophysics*, **42**, 295–301, 1999.

Turner, G. M., Toward an understanding of the multicomponent magnetization of uplifted Neogene marine sediments in New Zealand, *J. Geophys. Res.*, **106**, 6385–6397, 2001.

Turner, G. M., P. J. J. Kamp, A. P. McIntyre, S. Hayton, D. M. McGuire, and G. S. Wilson, A coherent middle Pliocene magnetostratigraphy, Wanganui Basin, New Zealand, *Journal of the Royal Society of New Zealand*, **35**, 197–227, 2005.

Veevers, J. J. and Z. X. Li, Review of sea-floor spreading around Australia. II Marine magnetic anomaly modelling, *Australian Journal of Earth Science*, **4**, 391–408, 1991.

Walbrecker, J. O., Records of geomagnetic polarity transitions from early Miocene sediments at Tarakohe Quarry, South Island, New Zealand, Grad. Dip. Sci. thesis, Victoria University of Wellington, New Zealand, 2005.

Walcott, R. I., Palaeomagnetically observed rotations along the Hikurangi Margin of New Zealand, in *Palaeomagnetic Rotations and Continental Deformation*, edited by C. Kissel and C. Laj, Kluwer Academic Publishers, 1989.

Wilson, G. S. and A. P. Roberts, Diagenesis of magnetic mineral assemblages in multiply redeposited siliciclastic marine sediments, Wanganui Basin, New Zealand, in *Palaeomagnetism and Diagenesis in Sediments*, edited by D. H. Tarling and P. Turner, Geological Society Special Publication 151, 1999.

G. M. Turner (e-mail: Gillian.Turner@vuw.ac.nz), D. M. Michalk, H. E. G. Morgans, and J. O. Walbrecker